Department of Chemical Engineering[1], Medicinal Plants and Drugs Research Institute, Shahid Beheshti University; Department of Animal Biology[2], School of Biology, College of Science, University of Tehran; Department of Agriculture[3], Medicinal Plants and Drugs Research Institute, Shahid Beheshti University, Tehran, Iran

Design and production of methyl jasmonate nanoemulsions using experimental design technique and evaluation of its anti-cancer efficacy

K. Habibi[1], H. Sepehri[2], L. Delphi[2], M. H. Mirjalili[3], H. Rafati[1,*]

Received April 30, 2017, accepted June 19, 2017

**Corresponding author: Dr. Hasan Rafati, Department of Chemical Engineering, Medicinal Plants and Drugs Research Institute, SB Univ., MPDRI, Velenjakm Shahid Beheshti University GC, Evin, Tehran, Iran*
h_rafati@sbu.ac.ir

Pharmazie 72: 652–662 (2017) *doi: 10.1691/ph.2017.7078*

Methyl jasmonate (MJ), a plant-derived stress hormone, has been shown to be a promising anti-cancer agent with high selectivity toward cancerous cells. The aim of the present study was to design a MJ loaded nanoemulsion (NE) to overcome the low MJ water solubility and also improve its anti-cancer efficiency. Box-Behnken design (BBD) was employed to optimize the composition effect of three independent manufacturing variables on two responses including average droplet size and poly dispersity index (PDI). ANOVA analysis indicated that both of the studied responses were well fitted by resultant quadratic models with the coefficient of determinations (R^2) 0.994 and 0.975, respectively. The actual average droplet size 75.06 nm and PDI 0.017 obtained for the optimum MJNE was in good agreement with those values predicted with numerical optimization. Physicochemical characterization indicated that the optimum MJNE was transparent, isotropic, spherical and sterically stabilized. MTT assay indicated that MJNE was more efficacious in killing cancer cells than MJ solution. Cell cycle analysis revealed that MJNE induced a stronger sub-G1 arrest than MJ solution. A considerable absence of toxicity was achieved for MJNE and blank NE in HUVEC normal cells. These results may provide strong support to develop a NE delivery system as a promising carrier for improving the safety and anti-cancer efficacy of MJ.

1. Introduction

Jasmonates are a class of plant stress hormones like salicylates, which are involved in regulation of many physiological events in plants (Wasternack 2014). For over 15 years, the most potent natural derivative of jasmonates i.e. methyl jasmonate (MJ) (Fig. 1), has been investigated for its potential anti-cancer effects in different types of preclinical cancer models such as breast, prostate, leukemia, melanoma, lung, colon and liver (Cesari et al. 2014). Different mechanisms of action have been suggested for the anti-cancer activity of MJ such as ATP depletion, detachment of hexokinase I and II from the mitochondria, re-differentiation induction, expression of reactive oxygen species, arrest of cell cycle, apoptosis induction and so on (Cesari et al. 2014). Interestingly, MJ acts selectively on cancerous cells without affecting normal cells (Rotem et al. 2005; Goldin et al. 2008). Since normal and cancerous cells differ in morphology and metabolism, those cancer therapies which act selectively on cancer cells have been attracted most investments worldwide (Ertel et al. 2006). However, the lipophilic nature (log p =2.76) and poor water solubility (0.1435 mg/mL at 25 °C) (Scognamiglio 2012) of MJ makes it difficult to dissolve it well in aqueous solution so its absorption and bioavailability is limited (Lipinski 2002).

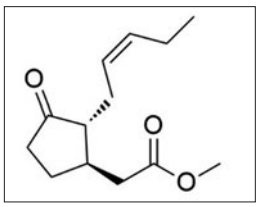

Fig. 1: Chemical structure of methyl jasmonate (methyl (1R, 2R)-3-oxo-2-(2Z)-2-pentenyl-cyclopentaneacetate)

Nanoemulsion (NE)-based delivery systems have been emerged as ideal carriers for the delivery of various hydrophobic drugs over the past years because of their outstanding advantages such as ease of preparation, enhanced solubilization and absorption, improved therapeutic efficacy, lowered adverse effect and toxic reactions (Jaiswal et al. 2015). NEs are colloidal dispersions of oil, water and surfactant usually in combination with a co-surfactant. HLB (hydrophilic-lipophilic balance) number and concentration of surfactant molecules were reported to have influential impacts on formation of stable emulsions with small average droplet size and low poly dispersity index (PDI) (Sagitani 1981). The ultrasonic emulsification technique which was employed in this study is reported as a fast and effective technique for preparation of NEs with very small droplet diameter and low PDI (Jafari et al. 2007; Kentish et al. 2008).

Since the traditional pharmaceutical formulation approach of one variable at a time is very laborious, cost and time consuming in drug development, statistical optimization techniques based on design of experiment (DOE) have been extensively employed to provide maximum information about the interactions between variables in a minimum number of runs (Rathore and Winkle 2009). Box-Behnken design (BBD) is a type of response surface methodology (RSM) that does not contain an embedded factorial or fractional factorial points and the design points fall at combinations of the high and low factor levels and also their midpoints. BBD has some advantages compared to the other experimental design of RSM such as the need for three levels of each factor and smaller number of the runs (Box and Behnken 1960).

Regarding the potential anti-cancer activity of MJ, the aim of the present study was to load MJ in a NE delivery system for improvement of its aqueous solubility and anti-cancer efficacy. To optimize

the different influential variables affecting the physical characteristics of NE formulations, BBD was employed. A further objective was to evaluate the anti-cancer activity of the optimized MJNE and its mechanism of action in MCF-7 cells. To the best of authors' knowledge, this study is the first report about the optimization and in vitro cellular evaluation of a NE-based delivery system of MJ.

2. Investigations, results and discussion

2.1. Model fitting and statistical analysis

The predicted and experimental values of the average droplet size and PDI responses are shown in Table 1. The response values obtained for the individual experimental runs were fitted into the design matrix. After evaluation of different statistical parameters, the software suggested the quadratic model to fit best for both the responses studied. ANOVA analysis of the resultant quadratic models is summarized in Table 2. Analysis of variance indicated that both the models were statistically significant with very low *p*-values ($p < 0.0001$) which indicated a satisfactory fitness of the models. Lack of fits with *p*-values greater than 0.10 indicated that there was significant difference compared to the pure error and both of the models were accurate for prediction of the response variables. The R^2 and adj-R^2 values close to 1.00 for both of the models suggested that more than 90 % of the variations in the response data could be explained by the models adequately. The values of adj-R^2 and pred-R^2 for two models were found to be within 0.2 of each other which demonstrated a good correlation between the experimental data and predicted values. Adequate precision, the ratio of signal to noise, greater than 4 indicated that both quadratic models are reliable. The C.V. values less than 10 % for two responses indicated no significant dispersion in data (Morgan 1991). The normal probability plots (normal % probability vs internally studentized residuals) indicated that data points distributed normally around the straight line with no outlier points (Fig. 2A). The respective correlation plots (predicted vs experimental data) demonstrated that the experimental responses are in good agreement with the predicted ones (Fig. 2B).

ANOVA results also showed that the linear terms of surfactant to oil ratio, HLB number and ultrasonic irradiation time followed by the quadratic terms of surfactant to oil ratio and HLB number were the most significant ($p < 0.0001$) effective variables on the average droplet size of MJNE. It was then followed by the quadratic term of ultrasonic time ($p < 0.001$) and then the interactive terms of ultrasonic time with either surfactant to oil ratio or HLB number ($p < 0.05$). For the PDI response, the most significant ($p < 0.0001$) effective term was the linear term of HLB number. The other significant terms were the linear term of surfactant to oil ratio and the quadratic term of HLB number ($p < 0.001$) then the quadratic terms of surfactant to oil ratio ($p < 0.01$) and ultrasonic time ($p < 0.05$). However, none of the interactive terms were noted to be significant on the PDI response. Since all of the linear terms were statistically significant, all of the respective quadratic and interactive terms should be included in the final models (Li and Chiang 2012). Therefore, the mathematical equations generated by MLRA for the responses studied should be written as the follows:

$$\text{Droplet size} = 510.55283 - 132.80071X_1 - 43.63729X_2 - 0.21825X_3 + 1.25091\,X_1X_2 - 0.068615X_1X_3 - 0.018602X_2X_3 + 28.55163X_1^2 + 1.63619X_2^2 + 1.29078 \times 10^{-3}X_3^2 \quad (1)$$

$$\text{PDI} = 0.16079 - 8.65044 \times 10^{-3}X_1 - 20.212 \times 10^{-3}X_2 - 6.49480 \times 10^{-5}X_3 - 3.03778 \times 10^{-4}X_1X_2 + 8.70508 \times 10^{-7}X_1X_3 + 1.60667 \times 10^{-6}X_2X_3 + 2.69551 \times 10^{-3}X_1^2 + 7.94608 \times 10^{-4}X_2^2 + 9.53731 \times 10^{-8}X_3^2 \quad (2)$$

Table 1: Scheme of BBD experimental design of predicted and experimental values of average droplet size (nm) and PDI

Run	Surfactant to Oil Ratio, X_1	HLB Number, X_2	Ultrasonic Time, X_3	Droplet Size (nm), Y_1		PDI, Y_2	
				Experimental	Predicted	Experimental	Predicted
1	1.65	8.00	30.00	129.29	128.05	0.038	0.037
2	1.65	14.00	300.00	45.19	46.45	0.016	0.016
3	0.30	14.00	165.00	141.12	141.08	0.026	0.025
4	0.30	8.00	165.00	197.22	203.09	0.042	0.041
5	3.00	14.00	165.00	59.48	53.62	0.014	0.015
6	1.65	14.00	30.00	86.57	91.23	0.019	0.018
7	3.00	8.00	165.00	95.32	95.37	0.035	0.035
8	3.00	11.00	300.00	51.31	55.94	0.019	0.018
9	0.30	11.00	30.00	187.85	183.24	0.029	0.030
10	1.65	11.00	165.00	57.34	56.53	0.016	0.017
11	1.65	11.00	165.00	50.91	56.53	0.019	0.017
12	1.65	8.00	300.00	118.04	113.40	0.032	0.032
13	1.65	11.00	165.00	55.55	56.53	0.018	0.017
14	1.65	11.00	165.00	57.07	56.53	0.015	0.017
15	0.30	11.00	300.00	179.71	178.53	0.025	0.025
16	3.00	11.00	30.00	109.47	110.66	0.022	0.021
17	1.65	11.00	165.00	61.74	56.53	0.016	0.017

Table 2: Analysis of variance and regression coefficients of the resultant quadratic models for the response variables

Source		Droplet Size (nm)				PDI			
	DF	SS	F-Value	P-Value		SS	F-Value	P-value	
Model	9	42980.80	151.15	< 0.0001	Sign.	0.001157	30.53	< 0.0001	Sign.
X_1	1	19044.84	602.77	< 0.0001		0.000127	30.20	0.0009	
X_2	1	5382.88	170.37	< 0.0001		0.000633	150.50	< 0.0001	
X_3	1	1768.20	55.96	< 0.0001		0.000030	7.15	0.0318	
X_1X_2	1	102.66	3.25	0.2894		0.000006	1.44	0.2695	
X_1X_3	1	625.51	19.80	0.0141		0.000000	0.024	0.8815	
X_2X_3	1	227.03	7.19	0.0441		0.000002	0.40	0.5461	
X_1^2	1	11400.75	360.83	< 0.0001		0.000102	24.14	0.0017	
X_2^2	1	913.03	28.90	< 0.0001		0.000215	51.15	0.0002	
X_3^2	1	2330.10	73.75	0.0005		0.000013	3.02	0.1257	
Residual	7	221.17				0.000029			
Lack of fit	3	160.56	3.53	0.1272	Not-Sign.	0.000008	0.47	0.7193	Not-Sign.
Pure Error	4	60.61				0.000022			
R^2					0.994				0.975
Adj-R^2					0.988				0.943
Pre- R^2					0.938				0.867
Adeq. precision					36.33				16.37
C.V.%					5.68				8.66

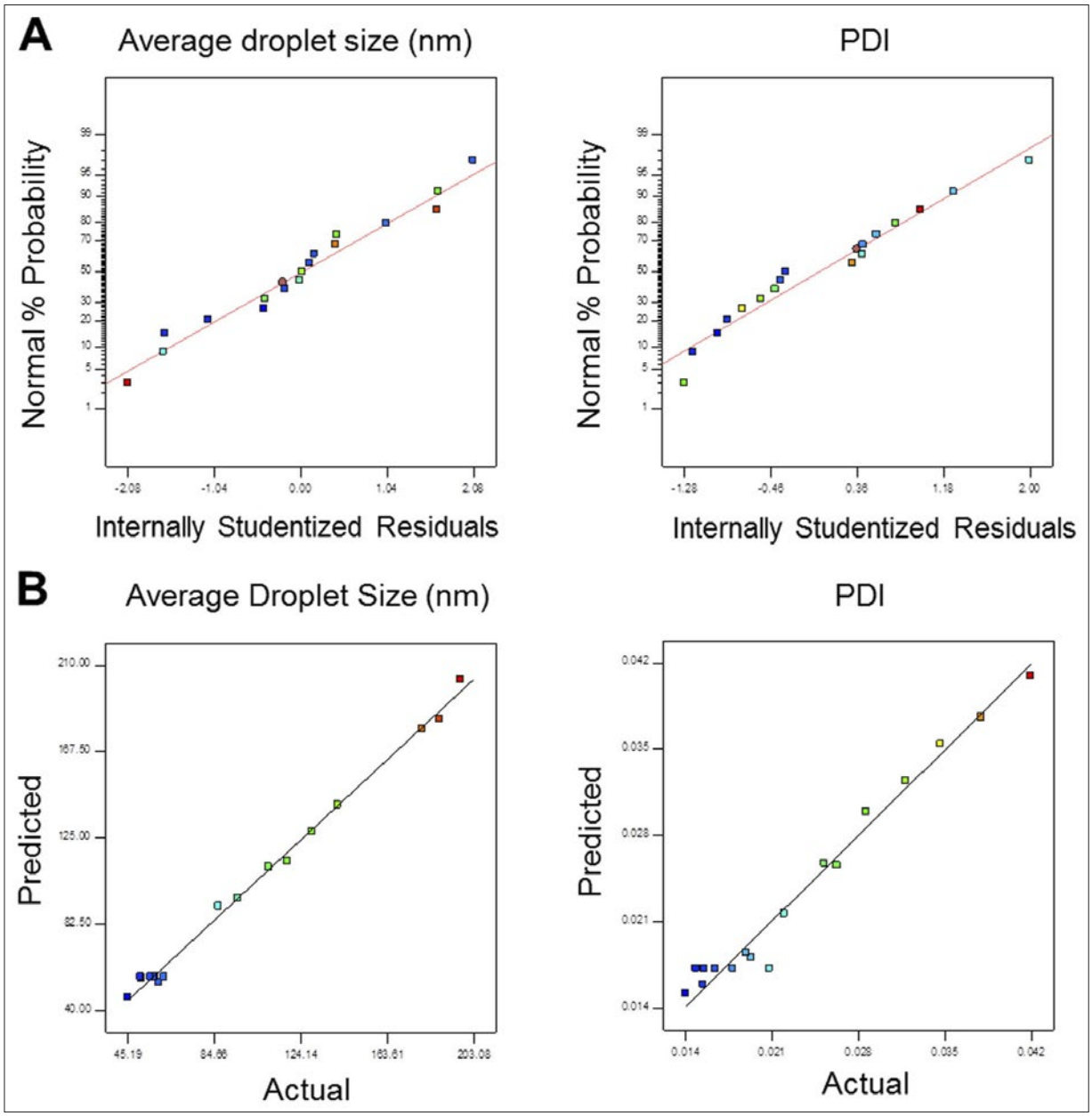

Fig. 2: Normal plots of residuals (A) and distribution plots of experimental vs predicted values (B) of the regression models of average droplet size and PDI

It should be noted that in both the quadratic models, coefficients with a positive sign represent a synergistic effect upon the responses while ones with negative signs represent an antagonistic effect. Inspection of Eq. (1) and (2) showed that both the average droplet size and PDI responses were negatively affected by the linear terms of three independently studied variables. In contrast, both responses were positively related to the quadratic terms of the independent variables which demonstrated that high levels of variables lead to an increase of average droplet size and PDI values.
On the other hand, any term in the models with a greater coefficient value would possess a more statistically significant effect on the respective responses (Morgan 1991). To visualize those independent variables that had the most influential impact on the respective responses, perturbation graphs were plotted (Fig. 3). A perturbation graph shows the effect of all independent variables at a special point in the design space. A steep slope or curvature in an independent variable shows that the response is sensitive to the respective variable. A relatively flat line shows insensitivity to the change in that particular variable (Sood et al. 2014). It was found that the surfactant to oil ratio and HLB number were the most influential variables on the average droplet size and PDI responses, respectively (Fig. 3).

2.2. Response surfaces analysis

To better visualize the interaction effects of independent variables on the responses studied, three-dimensional response surface plots and their corresponding contour plots were mapped with varying two of the independent variables in their respective experimental levels while the other one was kept constant at the central point.

2.2.1. Effect of independent variables on average droplet size response (Y_1)

Fig. 4 shows the combination effects of three independent variables on the average droplet size response. Interpretation of the 3-D plots and respective counter plots in Fig. 4 revealed that NEs with the smaller droplet size (<100 nm) were achieved at high concentration ratios of surfactant to oil. It was found that at the constant amount of oil, the average droplet size started to decrease by increasing the emulsifier concentration. This trend is in agreement with those earlier reports finding a reduction in the average droplet size with increasing the emulsifier concentration (Karadag et al. 2013; Musaa et al. 2013; Sood et al. 2014). As expected, at the high concentration ratio of surfactant to oil, the amount of surfactant molecules was entirely enough for formation

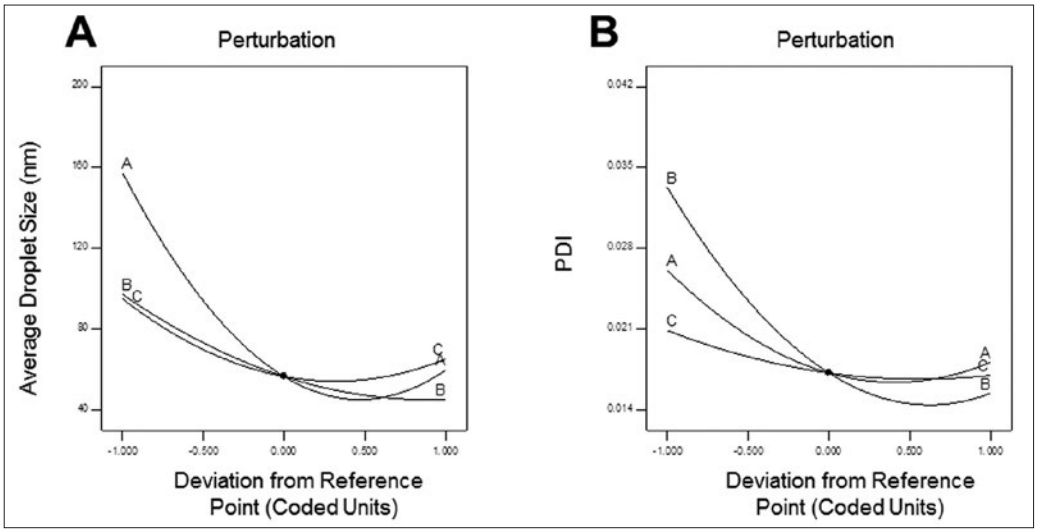

Fig. 3: Perturbation graphs for effect of surfactant to oil ratio (A), HLB number (B) and ultrasonic time(C) on average droplet size (A) and PDI (B)

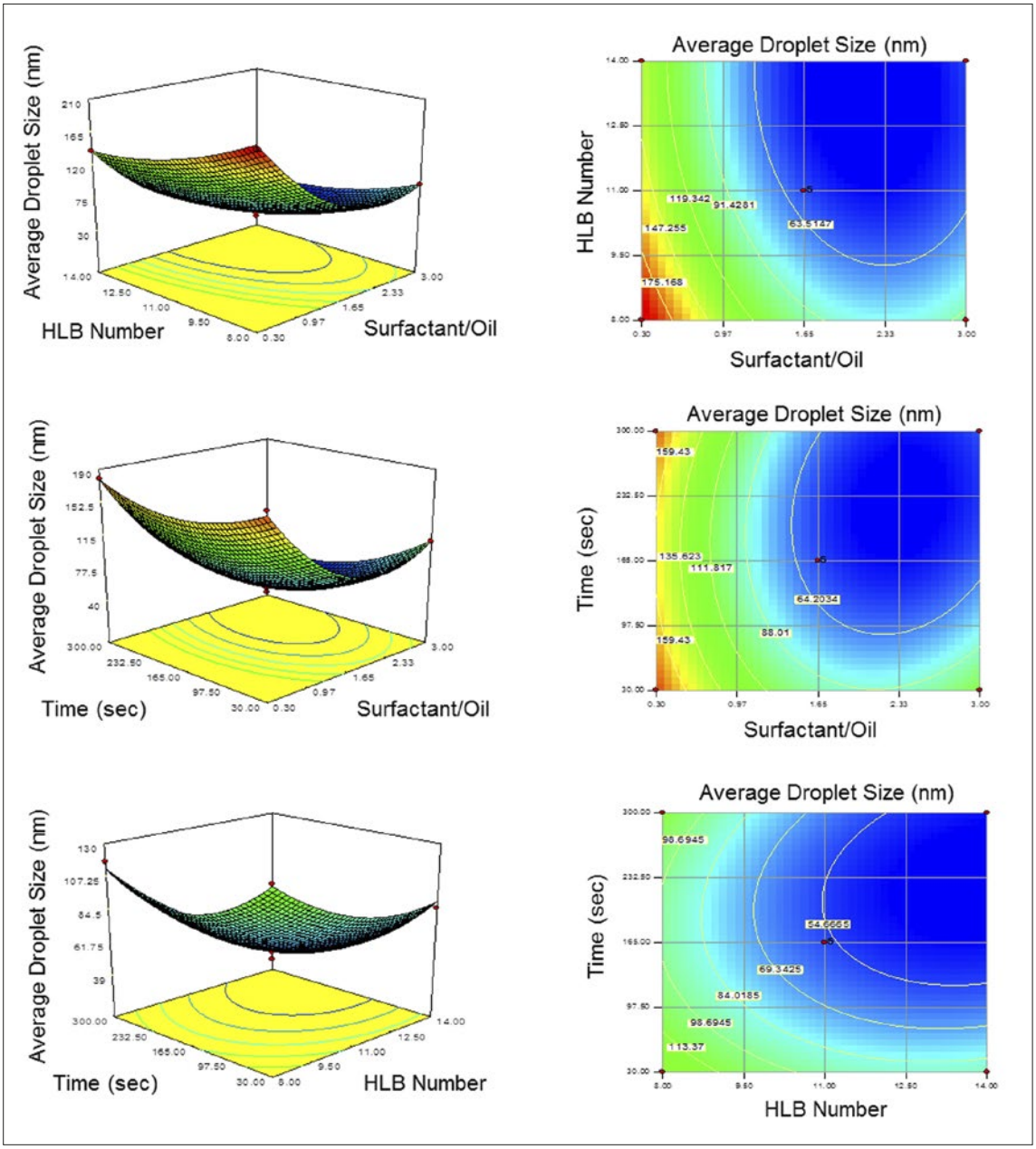

Fig. 4: Three dimensional surface plots and corresponding counter plots for effect of surfactant to oil ratio, HLB number and ultrasonic time on average droplet size

of an adsorbed monolayer onto the surface of newly formed oil droplets. Subsequently, the reduction of the interfacial tension between oil and water caused Laplace pressure and the overall droplet size decreased. In contrast, at a low ratio of surfactant to oil, the concentration of surfactant molecules was not sufficient for complete coverage of the temporary interface of oil-water interface, thus lowering the interfacial tension. At this condition, the break-up rate became restricted and oil droplets started to coalesce (Karadag et al. 2013; Musaa et al. 2013).

As shown in Fig. 4, smaller droplet sizes of NEs were achieved at high levels of HLB number. It was found that the average droplet size of NEs did not change significantly by increasing the mass percentage of Span 80 in combination mode with Tween 80 up to HLB number of 12, while below this value the average droplet size started to increase dramatically by increasing the concentration of Span 80. This could be caused by the fact that increasing the concentration of Span 80 as a lipophilic surfactant may make the emulsion system too hydrophobic. Therefore, the stability of the emulsification system would be deteriorated and cause the overall droplet size to increase (Leong et al. 2009).

It was also found that besides the concentration of emulsifier and the HLB number, the final average droplet size of nanoformulations was also controlled by the time of exposing to ultrasonic waves. Arguably, the shear force which is also expressed as the energy density (E_v) is related conversely with the average droplet diameter (d_{av}) with a simple exponential equation (Eq. (3)):

$$d_{av} = C \cdot E_v^{-b} \quad (3)$$

The energy density (E_v) is the simple product of the power density (P_v) and the irradiation time (t) within the applied shear field (Eq. (4)):

$$E_v = P_v \cdot t \quad (4)$$

From the Eq. (3) and (4), it is revealed that the average droplet size is also correlated inversely with the irradiation time as an increase in the irradiation time leads to an increase of the energy density following decrease of the average droplet size (Leong 2009).

2.2.2. *Effect of independent variables on PDI response (Y_2)*

The combination effects of the independent variables on the PDI response are shown in Fig. 5. As observed, NEs with narrow PDI values were achieved at high ratios of surfactant to oil, high HLB numbers and long ultrasonic time. As discussed for the average

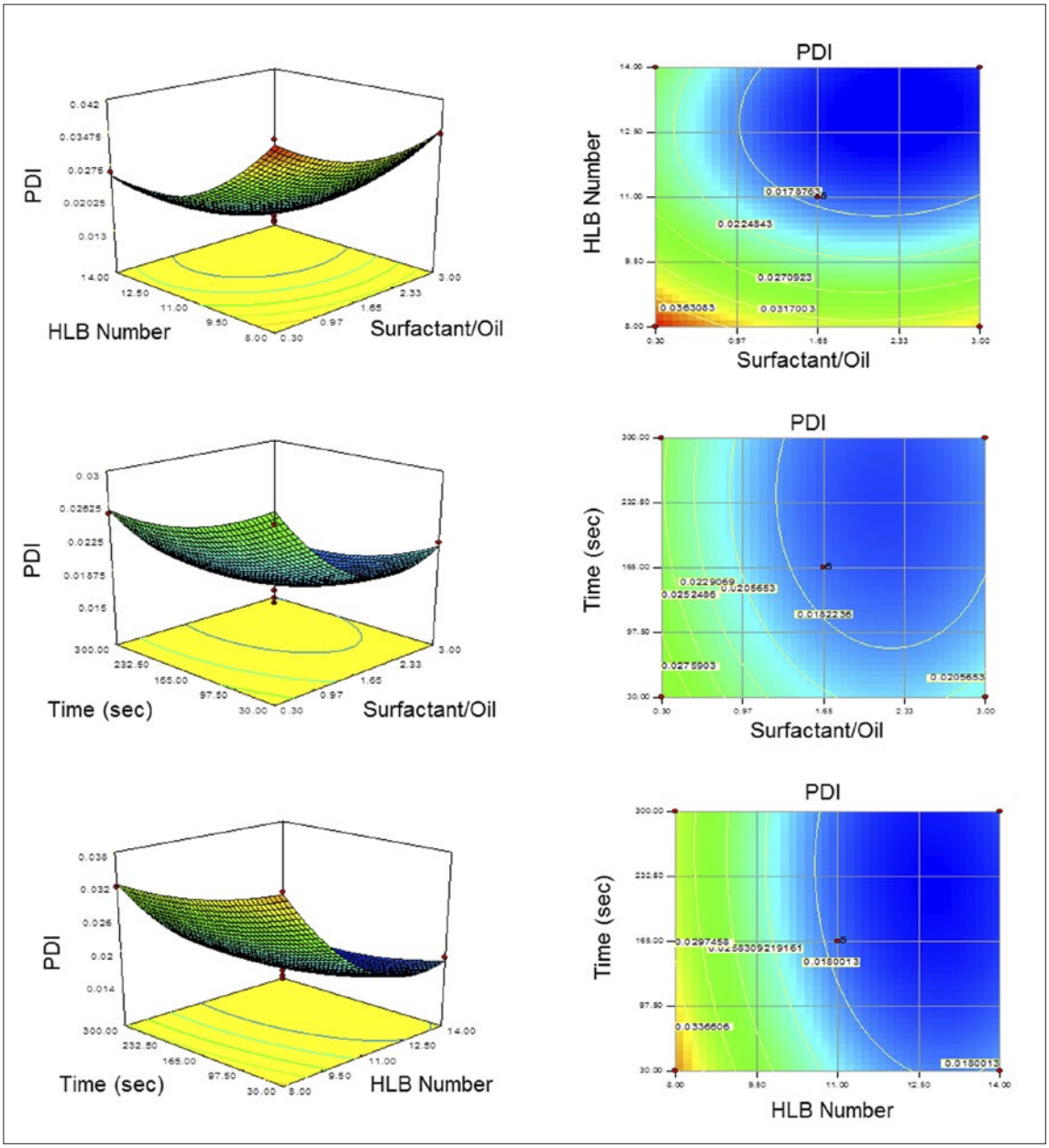

Fig. 5: Three dimensional surface plots and corresponding counter plots for effect of surfactant to oil ratio, HLB number and ultrasonic time on PDI

droplet size response, a high concentration of surfactant molecules could ease the droplet break-up process by lowering the interfacial tension of the oil-water interface and result in formation of stabilized droplets with narrow droplet size distribution (Karbstein and Schubert 1995; Morales et al. 2003). It was also found that PDI values decreased by reducing the HLB number from 14 to 8. Similar to the trend achieved for the average droplet size response, it might be due to the higher concentrations of Span 80 in the emulsion batch system, which decreased the stability of emulsification system (Leong 2009). In addition, increasing the irradiation time caused PDI values to decrease. Reduction of PDI values by increasing the irradiation time is in agreement with the previous studies (Abismail et al. 1999; Tan et al. 2016). As a rule, longer irradiation time will increase the temperature of the emulsification batch system and results in the reduction of interfacial tension and the viscosity of the oil phase. It leads to the formation of a homogenous system with narrow droplet size distribution (Gaikwad and Pandit 2008). However, in the case that irradiation time exceeds a particular range, it will lead to the temperature elevation of the emulsification batch system and results in the instability of the nanoemulsions (Abismail et al. 1999).

2.3. Optimization and model verification

In order to achieve an optimized MJNE with the minimum values of average droplet size and PDI using the numerical optimization method, the levels of all independent variables were set within the specified range except the value of surfactant to oil ratio which was set at 1:1. Indeed, the application of a high surfactant concentration in drug formulations is not desirable in pharmaceutical industry due to the potentially toxic effects of surfactant molecules and also cost ineffectiveness (Ahmad et al. 2014; Han et al. 2009). Eventually, the combined ingredient levels of surfactant to oil ratio 1:1, HLB number 12.70 and ultrasonic time 163.62 s with the maximum desirability function 1 was selected as the optimum composition for the average droplet size and PDI responses. In order to check the adequacy and validity of the final models, the predicted values and the experimental data obtained for both responses were compared with computing their respective RSE (%). As shown in Table 3, the RSE (%) values of average droplet size and PDI were 7.2 and 5.5. The small percentage error revealed good agreement between the experimental data and predicted values which verified the BBD ability for optimization of the physicochemical characteristics of MJNE.

Table 3: Predicted and experimental response values of optimum MJ nanoemulsion

Run	Surfactant to Oil Ratio	HLB Number	Ultrasonic Time (sec)	Droplet Size (nm)		PDI	
				Experimental	Predicted	Experimental	Predicted
1	1	12.70	163.62	75.06	80.86	0.017	0.018

2.4. Emulsion characterization

Understanding the physicochemical characteristics of formulations and integrating this knowledge with the biopharmaceutical properties is essential for formulation development and the ultimate performance of the drug product. Thus, different physicochemical characterizations of optimized MJNE were carried out and results obtained were summarized in Table 4.

Table 4: Physicochemical properties of the optimum MJ nanoemulsion

Physicochemical Parameter	Value
Appearance	Transparent
Zeta potential (mV)	- 0.342
Surface tension (mN m^{-1})	26.65
Percentage transmittance (%)	99.70
Refractive index	1.335
Viscosity (cP)	2.5
Droplet shape	Spherical
Storage stability	No phase seperation

The zeta potential is a measure of the electric charge at the interface between a particle surface and its liquid medium. It is generally accepted that colloids with a high value of zeta potential (ZP > |30|) are electrically stabilized while the colloids with low zeta potential tend to coalesce or aggregate (Barradas et al. 2014). However, there are some reports that demonstrated the low values of zeta potential did not have a drawback effect on nano-droplets stability (Kakumanu et al. 2011; Zhu et al. 2015). The average zeta potential value measured for the optimized MJNE was – 0.342 mV. The low surface charge value obtained for MJNE is rational because both emulsifiers utilized were non-ionic surfactants and the negligible negative charge observed is due to the hydrogen bonding between the ethylene oxide groups of Tween 80 molecules and hydroxyl groups of water molecules at the interfacial layer (Liu et al. 2006). The low surface tension value obtained for the optimized formulation (26.65 mN/m) was attributed to the surfactant mixtures which reduced the oil-water surface tension adequately.

The value of percentage transmittance (99.7 %) close to 100 % verified that the optimized formulation was transparent.

Refractive index is an optical property which can be used to characterize the isotropic nature of the emulsions. Refractive index values measured for the optimal NE (1.335) indicated that NE remained isotropic in nature and had no drug excipient interactions. Also, the value was very close to the refractive index value of water (1.330) which demonstrated the oil-in-water behavior of the emulsion formulation (Alanazi et al. 2013). The optimized formulation showed a non-Newtonian behavior and the measured maximum viscosity (2.5 mPas) was very low which is expected for NEs.

In order to verify the DLS data and obtain details about the shape of emulsion droplets, transmission electron microscopy was performed. TEM due to direct visualization of particles has the potency to supply more accurate information about the size and specially the shape of the particles. As is shown in Fig. 5, the droplets of MJNE appeared as bright droplets in a dark surrounding area. Their shape was spherical. The droplet size distribution was nearly mono-dispersed and the estimated size (less than 100 nm) was in good agreement with the results obtained by the particle size analyzer (DLS).

Visual inspection indicated that the optimal MJNE was physically stable without any visible sedimentation, creaming and flocculation through the testing period. The stability profile of droplet size and PDI at two temperatures of 4 and 25 ºC over a period of one month are shown in Fig. 6. The average droplet size of MJNE stored at 4 °C was nearly constant while the average droplet size of nanoemulsion stored at 25 °C grew steadily through the time. The PDI value at both temperatures increased and this increment was more evident at 25 °C compared to 4 °C. However, the average droplet size and PDI values were still in favorable ranges i.e. around 100 nm and less than 0.05. Although the zeta potential value of the optimized MJNE was less than |30| mV, the formulation was stable enough and no phase separation was observed. This could be explained by the sufficient steric stabilizing effect

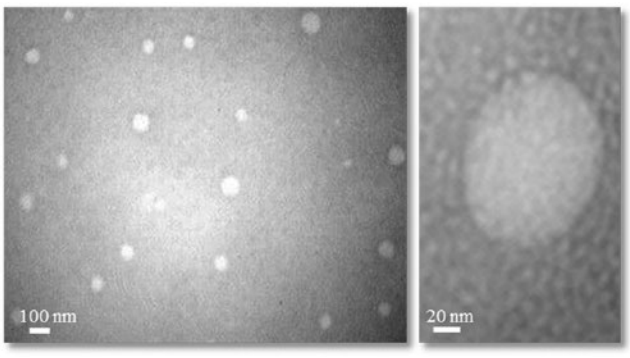

Fig. 6: Transmission electron micrograph (TEM) negative image of droplets of optimum MJNE at two scales

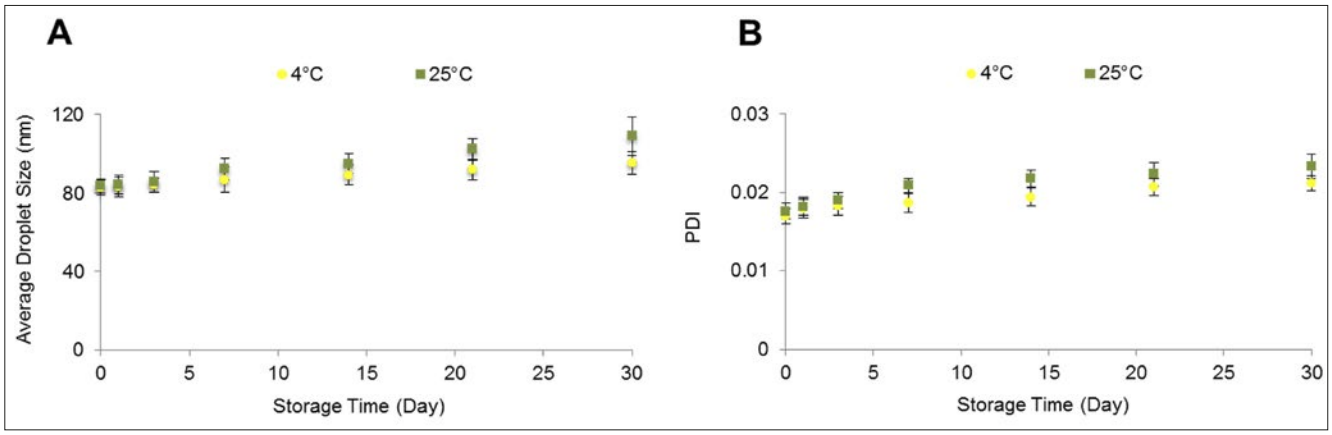

Fig. 7: Storage stability profiles of average droplet size (A) and PDI (B) of optimum MJNE at two temperatures 4 and 25 °C

of the non-ionic surfactant mixtures i.e. Tween 80 and Span 80 which formed a strong steric barrier around the dispersed droplets and prevented their coalescence (Loong et al. 2014). However, the growth in the diameter and PDI of the droplets at higher temperature i.e. 25 °C may be due to the Ostwald ripening effect which is a temperature sensitive process and considered the main mechanism of NEs instability (Karbstein and Schubert 1995; Tadros et al. 2004; Sood et al. 2014). On the other hand, at higher temperatures, the Brownian motion of the oil droplets and the collision between them will increase which could result in droplets coalescence (Eid et al. 2013). From the results, the temperature of 4 °C is a preferred storage condition for the optimized MJNE which are stabilized with a minimum concentration of non-ionic surfactant mixtures (1 : 1 (w/w) ratio of MJ and surfactant mixtures).

2.5. Cell proliferation assay

The effect of MJ solution and MJNE on MCF-7 cell proliferation using concentrations of 1.0, 1.5 and 2.0 mM are shown in Fig. 8. Based on MTT assay results, the viability of cells treated

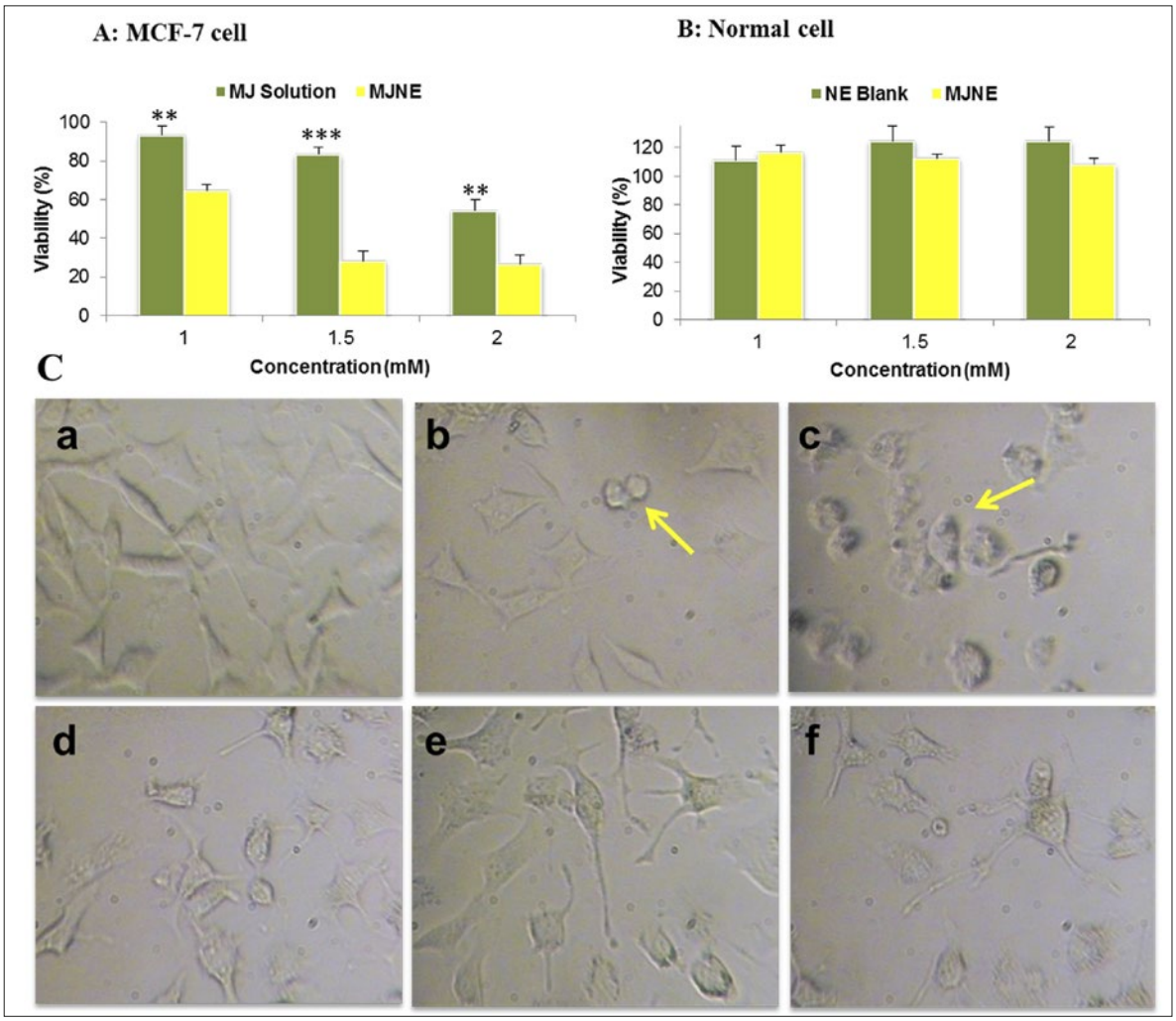

Fig. 8: Viability (%) of MJ solution and NE in MCF-7 cells (A) and blank NE and MJNE in HUVEC cells (B) after 24 h treatment at three different concentrations. (C) Morphological observations of MCF-7 and HUVEC cells upon treatment with 2 mM concentration of MJ solution, NE and blank NE. Fig a, b and c depict MCF-7 control cells, treated with MJ solution and NE, respectively. Fig d, e and f depict HUVEC control cells, treated with blank and MJNE, respectively. (*), (**) and (***) indicate the statistical significance difference with p-values < 0.05, 0.01 and 0.001, respectively. (Data analyzed statistically by two-tailed Student's t-test)

with MJNE at doses of 1.0, 1.5 and 2.0 mM were 64.72, 28.36 and 26.48 %, whereas those of MJ solution were 93.15, 83.2 and 54.03%, respectively. In this way, inhibition percentages in MJNE were 5.1, 4.3 and 1.6 times more than the MJ solutions. In addition, the NE without MJ as blank sample did not change cells viability (data not shown). It was found that MJ in the form of NE induced more proliferating inhibition than MJ solution in all concentrations and the observed differences were statistically significant. It might be due to the enhanced solubility as well as uptake of MJ into the cancer cells in the form of NE (Lin et al. 2014). These data are in agreement with earlier studies reporting that the drug loaded in the NE vehicle showed a greater cytotoxic effect on cancer cells in comparison to the free drug (Ganta and Amiji 2009; Sharma et al. 2015). As seen in Fig. 8, MJNE and blank NE did not significantly affect the HUVEC's viability. As the safety of a newly introduced delivery system is very important for pharmaceutical applications, these data could demonstrate the MJNE play their specific role on cancerous cells without affecting normal cells.

The morphological changes in MCF-7 cells treated with MJ solution and NE were studied. As can be observed in Fig. 8, the morphological changes revealed as floating round compressed cells in comparison to the control cells. Treatment of the MCF-7 cells with 2 mM concentration of MJNE showed the most granule and detached cells in comparison to the control as well as those cells treated with MJ solution. Conversely, the morphological features of the HUVEC cells did not reveal any dominant changes (Fig. 8). The same morphological changes were also reported by Tamimi et al. (2016).

2.6. Nuclear morphological changes

Hoechst staining is a classical method to observe the nuclear morphology of apoptotic cells. It was shown that nuclei of most MCF-7 cells treated with MJNE were stained highly condensed, with bright nucleus; while the cells in control group and MJ solution treatment were stained slightly blue. As shown in Fig. 9 the apoptotic features in MJNE treated cells more prominent than those of MJ solution alone.

2.7. Cell cycle analysis with flow cytometer

Further, cell cycle analysis was done to investigate whether MJNE induced apoptosis. At the late steps of apoptosis, aggregation of fragmented DNA into low molecular weight oligomers occurred. Therefore, apoptotic cells included a hypodiploid or 'sub-G1' peak in a DNA histogram (Clyburn et al. 2010). Figure 10 demonstrates that control group and the cells treated with the blank NE did not contain high peaks in sub-G1 region (lower than 5%), while MJ and MJNE showed high peak intensity in this area. In addition, the data displayed that MJNE induced a stronger sub-G1 cell arrest in comparison to the MJ treated cells.

4. Experimental

4.1. Materials

MJ (p = 1.03 g/mL, RI = 1.474) was purchased from Sigma-Aldrich Chemie GmbH, Germany. Sorbitan monooleate (Span 80) and polyoxyethylene sorbitan monooleate (Tween 80) were obtained from Merck Millipore, Darmstadt, Germany. Deionized and Milli-Q (Millipore Corporation, Molsheim, France) filtered water was used in all experiments. PRMI medium and MTT (3-(4,5-dimethylthiazol-2yl)-2,5- diphenyltetrazoliumbromide) for cell culture studies were bought from Sigma Aldrich (St Louis, MO, USA). Penicillin–streptomycin and fetal bovine serum (FBS) were obtained from Gibco (Gibco, Grand Island, NY, USA).

4.2. Preparation of nanoemulsion

MJ loaded NE was formulated with non-ionic surfactant mixtures consisting of Tween 80 (hydrophilic, HLB number: 15, interfacial molecular area: 2.48 nm^2) and Span 80 (lipophilic, HLB number: 4.3, interfacial molecular area: 0.46 nm^2). Generally, application of surfactants with opposing HLB numbers and molecular packing parameters can improve the interfacial curvature of oil-water mixture and causes the reduction of interfacial tension due to surfactant synergy (Leong et al. 2009). Different mixtures of Tween 80 and Span 80 were prepared to obtain the optimum weight ratio. The HLB value of the surfactant mixtures (HLB_{mix}) were measured using the following equation (Eq. (5)):

$$HLB_{mix} = f_a\, HLB_a + f_b\, HLB_b \quad (5)$$

where HLB_a and HLB_b are the HLB values of Tween 80 and Span 80, f_a and f_b are the weight fractions of Tween 80 and Span 80, respectively. For preparation of oil-in-water NE loaded with MJ, Tween 80 was dissolved in deionized water and Span 80 was dissolved in MJ. An initial dispersion was produced following the addition of aqueous phase into the oil phase. Then, the resulting dispersion was treated ultrasonically by a 20 kHz ultrasonic processor operating at amplitude of 30% and nominal power of 400 W (MPI, Rue du Marais 36, 2400 Le Locle, Switzerland). In all experiments, the horn microtip with 3 mm diameter was symmetrically dipped into the emulsification batch at a repeatable depth of 2 mm. The temperature difference between the initial and final emulsion batch was not more than 20 ºC under the studied operating conditions.

4.3. Experimental design and statistical analysis

A three-level, three-factor BBD was employed to statistically optimize the composition effect of three independent variables including surfactant to oil ratio (0.3-3, x_1), HLB number (8-14, x_2) and ultrasonic time (30-300 s, x_3) on the two response variables namely the average droplet size (Y_1) and PDI (Y_2). According to the preliminary experiments, the independent variables and their influential levels were selected. Design-Expert® 7.0.0 software (Stat-Ease Inc., Minneapolis, USA) proposed 17 experimental runs in according to BBD with five replicates of center points. Individual experiments were done in randomized order to minimize the effect of uncontrolled variables on the response variables. The coded and uncoded independent variables used in BBD are shown in Table 5.

Table 5: Coded levels for independent variables used in 3-level-3-factor Box-Behnken design

Independent variables	Unit	Coded levels		
		-1	0	+1
Surfactant to Oil Ratio, X_1	-	0.30	1.65	3.00
HLB Number, X_2	-	8.00	11.00	14.00
Ultrasonic Time, X_3	second	30.00	165.00	300.00

Multiple linear regression analysis (MLRA) was applied to determine the coefficients of polynomial regression model of two responses studied with the following mathematical equation (Eq. (6)):

$$Y_i = \beta_0 + \sum_{i=1}^{3} \beta_i x_i + \sum_{i=1}^{3} \beta_{ii} x_i^2 + \sum_{i=1}^{2} \sum_{j=i+1}^{3} \beta_{ij} x_i x_j \quad (6)$$

where Y_i is the predicted response; β_0 is a constant term; β_i, β_{ii} and β_{ij} are the linear, quadratic and interactive coefficients, respectively; x_i and x_j are the codes of independent variables. Analysis of variance (ANOVA) was applied to estimate the statistical significance of regression coefficients and regression models. The degree of fitness of both the resultant models was evaluated by coefficients of determination (R^2), adjusted coefficients of determination (adj-R^2), predicted coefficients of determination (pred-R^2), lack of fit, coefficient of variance (C.V.%) and adequate precision. These statistical parameters were also used to choose the best-fitting mathematical model. Eventually, a final model was generated for each response variable in according to significance value ($p < 0.05$) of each regression coefficient (Morgan 1991).

4.4. Optimization and model verification

Numerical optimization method of the Design Expert® software was employed to get a final formulation with desired response variables. The lower and upper limits of three independent variables were set and an optimum composition was selected based on the criteria of maximum desirability function among the different recommended compositions by the software. To verify the adequacy of the final models, the experimental values obtained for optimum formulation were compared with the predicted ones by calculating the percent of residual standard error (RSE %) with the following equation (Eq. (7)) (Loong et al. 2014) :

$$RSE(\%) = \frac{Exp.value - Pre.value}{Pre.value} \times 100 \quad (7)$$

4.5. Characterization of NE

4.5.1. Average droplet size and PDI measurement

The hydrodynamic diameter (Z-average) and PDI of the NEs were measured using a dynamic light scattering (DLS) particle size analyzer (Nanophox, Sympatec, Germany) equipped with an argon laser operating at 633 nm and a high-sensitivity avalanche photodiode detector. All measurements were carried out at fixed angle of 173º and room temperature of 25.0±0.5 ºC. A refractive index of 1.474 was used for MJ in Mie theory calculations. Dynamic light scattering measures the intensity fluctuation of scattered light which resulted from Brownian motion of nano-sized droplets in emulsions. The resultant value for Brownian motion is related to the particle size and viscosity of the dispersing agent (Stepanek 1993). Accordingly, nanoformulations were diluted to a scattering intensity of less than 2000 kcps to avoid the undesirable effects of multiple scattering and viscosity. The second important parameter PDI, a dimensionless measure of the width of the particle size distribution, was calculated

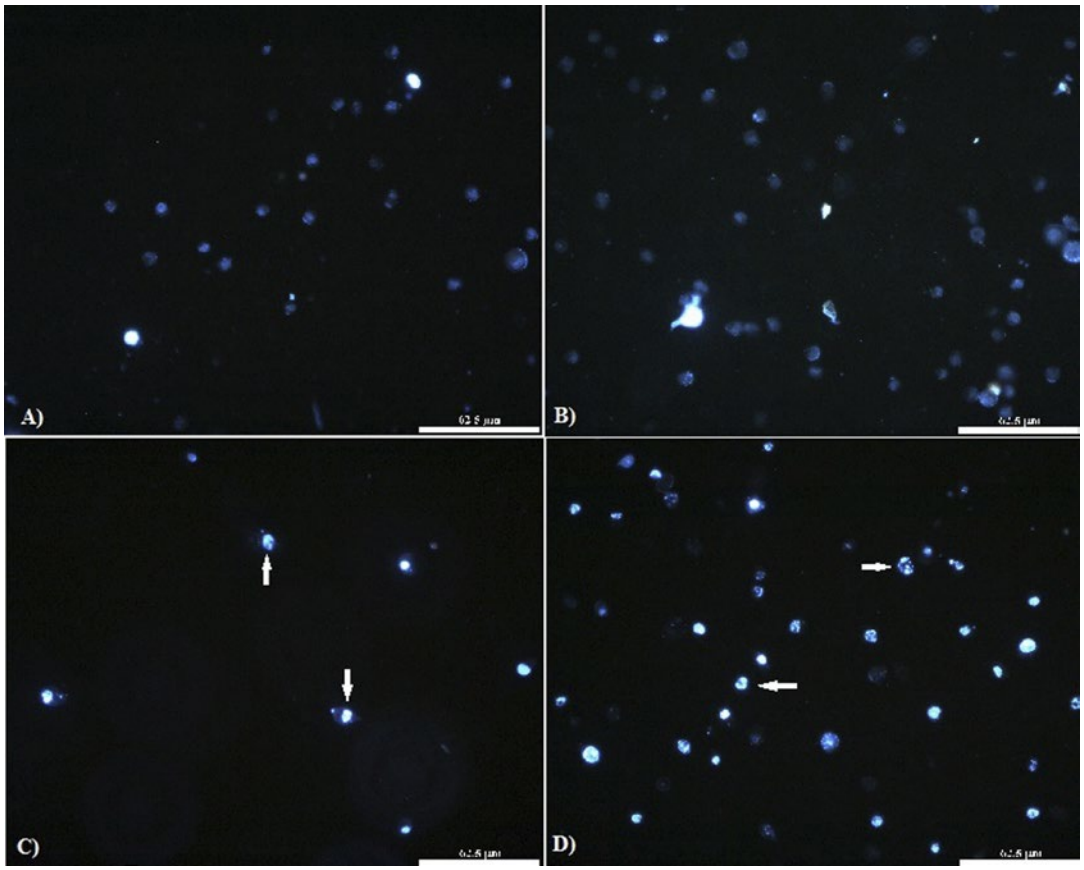

Fig. 9: Nuclear morphological changes in MCF-7 control cells (A) upon treatment with Blank NE (B) MJ solution (C) and MJNE (D) at 2mM concentration after 24 h. Arrows shows condensed and fragmented nuclei

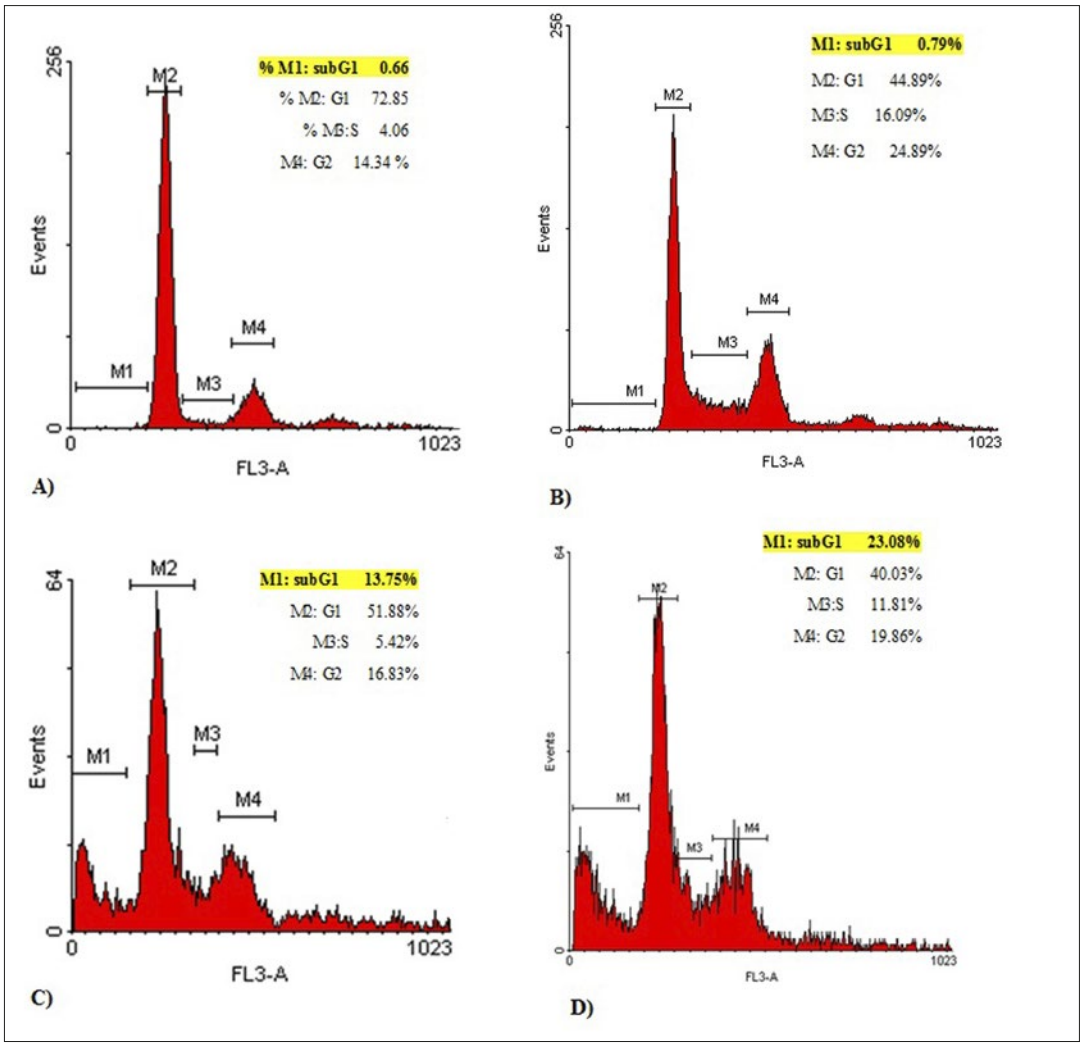

Fig. 10: Cell cycle arrest in MCF-7 control cells (A) upon treatment with Blank NE (B) MJ solution (C) and MJNE (D) at 2mM concentration after 24 h

from the cumulant analysis. PDI less than 0.05 are typically referred as monodispersed population (Hackley and Ferraris 2001).

4.5.2. Zeta potential

Analysis of surface charge was done using Zetasizer (Nano ZS, Malvern Instrument, UK) at room temperature. The formulation was diluted and placed in the electrophoretic cell of the instrument. Zeta potential was calculated by measuring the electrophoretic mobility of dispersed droplets in a charged field.

4.5.3. Surface tension

Surface tension of the optimum formulation was measured using tensiometer (K100, KRUSS, Hamburg, Germany) at room temperature with drop shape analysis method.

4.5.4. Percentage transmittance

Percentage transmittance of the optimum formulation was assessed by UV-160A double beam spectrophotometer (Shimadzu, Japan). The formulation was diluted 100 times using water and analyzed at 638.2 nm (Loong et al. 2014).

4.5.5. Refractive index

Refractive index of the optimized formulation was assessed at 25 °C using an Abbe type refractrometer (Bausch and Lomb Optical Company, Rochester, NY) without any dilution.

4.5.6. Viscosity

Viscosity of the optimized NE was performed at 25 °C using a MCR 502 rheometer (Anton Paar GmbH, Graz, Austria) with the parallel plate (PP50) configuration. For analysis, 2 mL of the emulsion was loaded onto the rheometer without dilution. The viscosity of NE was measured by the steady state flow program with the shear rate in the range of 100-1000 per seconds during 5 min.

4.5.7. Transmission electron microscopic (TEM) analysis

The morphology of optimized NE loaded with MJ was visualized using transmission electron microscopy (TEM). A drop of emulsion was placed on 300-mesh formwar-coated copper. The sample was then negatively stained with 2.0 % uranyl acetate and was dried at room temperature. Excess liquid was dabbed with a piece of Whatman filter paper. The TEM samples were observed with a transmission electron microscope (EM10C, Zeiss, USA) operating at 80 kV.

4.5.8. Stability studies

The physical stability of the optimized formulated MJNE was monitored by measuring the average droplet size and PDI during different interval times up to one month storage at two different temperature conditions i.e. 4 and 25 ºC using dynamic light scattering. The measurements were triplicated and reported as the mean values±SD.

4.6. Cell proliferation assay

The MTT assay was carried out on human breast carcinoma cell (MCF-7) and normal cells (HUVEC). Both MCF-7 and HUVEC cell lines were obtained from the Pasteur Institute (Tehran, Iran). The cells were grown in RPMI medium contained 10% fetal bovine serum and 1% antibiotic mixture comprising penicillin-streptomycin in a humidified atmosphere at 37 °C with 5% CO_2. Growth medium was changed three times a week and when they reach 70-80% confluence, the medium was subcultured again. Cells were plated in 96-well plate and incubated overnight. After that the MCF-7 cells were treated with different doses of MJ solution, MJNE and blank NE (1, 1.5 and 2 mM) for 24 h. To study the safety of the optimized nanoformulation, MJNE and blank NE were treated to HUVEC cells at the same dose (1-2 mM) and incubation time (24h).
Cell morphology was observed and photographed using an optical microscope (CETI, Belgium) equipped with a digital camera. Cell toxicity was determined by the conventional MTT reduction assay (Chauhan et al. 2005). The dark blue formazan crystals formed in intact cells were solubilized in dimethyl sulfoxide and the absorbance was measured at 630 nm. The viability (%) was calculated from the following equation (Eq. (8)):

$$\text{Viability}(\%) = \left(\frac{A_{treated}}{A_{control}}\right) \times 100 \quad (8)$$

4.7. Nuclear morphological changes by Hoechst 33258 staining

The MCF-7 nuclear morphological changes were observed with Hoechst 33258 staining. Briefly, the cells were treated with MJ solution, MJNE and blank NE for 24 h. Then cells were collected, washed in PBS (pH 7.4) and stained with 10 µg/mL of Hoechst 33258 for 5 min. Finally, the cells were observed using a fluorescence microscope (Zeiss, Germany). Apoptotic cells characterized by chromatin fragments were counted in five random fields for each group of cells.

4.8. DNA cell cycle analysis by flow cytometry

1×10^6 cells were treated with MJ solution, MJNE and blank NE for 24 h, the untreated and treated cells were harvested, washed and fixed in cold alcohol, then the cells were treated with 100 µg/L RNase in PBS, followed by staining with 20 mg/L propidium iodide. The apoptosis rate was indicated by the percentage of cells in the sub-G1 fraction, using flow cytometer using WinMDI software.

Acknowledgements: This research was supported by the Shahid Beheshti University Research Council and the authors gratefully acknowledge the support provided by MPDRI.

Conflicts of interest: None declared.

References

Abismail B, Canselier JP, Wilhelm AM, Delmas H, Gourdon C (1999) Emulsification by ultrasound: drop size distribution and stability. Ultrason Sonochem 6: 75-83.
Ahmad J, Mir SR, Kohli K, Amin S (20140 Effect of oil and co-surfactant on the formation of Solutol HS 15 based colloidal drug carrier by Box-Behnken statistical design. Colloids Surf A 453: 68-77.
Alanazi FK, Haq N, Radwan AA, Alsarra IA, Shakee F (2015) Formulation and evaluation of cholesterol-rich nanoemulsion (LDE) for drug delivery potential of cholesteryl-maleoyl-5-fluorouracil. Pharm Dev Technol 20: 266-270.
Barradas TN, Campos VE, Senna JP, Coutinho C, Tebaldi BS, Silva K, Mansur C (2014) Colloids Surf A 480: 214–221.
Box GEP, Behnken DW (1960) Some new three level designs for the study of quantitative variables. Technometrics 2: 455-475.
Chauhan D, Li G, Podar K, Hideshima T, Neri P, He D, Mitsiades N, Richardson P, Chang Y, Schindler J, Carver B, Anderson KC (2005) A novel carbohydrate-based therapeutic GCS-100 overcomes bortezomib resistance and enhances dexamethasone-induced apoptosis in multiple myeloma cells. Cancer Res 65: 8350-8358.
Cesari IM, Carvalho ME, Figueiredo R, Mendonça BS, Dias AN, David RF (2014) Methyl jasmonate: putative mechanisms of action on cancer cells cycle, metabolism, and apoptosis. Int J Cell Biol 1: 572097.
Clyburn RD, Reid P, Evans CA, Lefley DV, Holen I (2010) Increased anti-tumour effects of doxorubicin and zoledronic acid in prostate cancer cells in vitro: supporting the benefits of combination therapy. Cancer Chemother Pharmacol 65: 969-978.
Eid AMM, Elmarzugi NA, El-Enshasy HA (2013) Preparation and evaluation of olive oil nanoemulsion using sucrose monoester. Int J Pharm Pharm Sci 5: 434-440.
Ertel A, Verghese A, Byers SW, Ochs M, Tozeren A (2006) Pathway-specific differences between tumor cell lines and normal and tumor tissue cells. Mol Cancer 5: 55.
Gaikwad SG, Pandit AB (2008) Ultrasound emulsification: effect of ultrasonic and physicochemical properties on dispersed phase volume and droplet size. Ultrason Sonochem 15: 554-563.
Ganta S, Amiji M (2009) Coadministration of paclitaxel and curcumin in nanoemulsion formulations to overcome multidrug resistance in tumor cells. Mol Pharm 6: 928-939.
Goldin N, Arzoine L, Heyfets A, Israelson A, Zaslavsky Z, Bravman T, Bronner V, Notcovich A, Shoshan-Barmatz V, Flescher E (2008) Methyl jasmonate binds to and detaches mitochondria-bound hexokinase. Oncogene 27: 4636-4643.
Hackley VA, Ferraris CF (2001) The use of nomenclature in dispersion science and technology. Recommended Practice Guide, National Institute of Standards and Technology (NIST) Washington.
Han M, He CX, Fang QL, Yang XC, Diao YY, Xu DH, He QJ, Hu YZ, Liang WQ, Yang B, Gao JQ (2009) A novel camptothecin derivative incorporated in nano-carrier induced distinguished improvement in solubility, stability and anti-tumor activity both in vitro and in vivo. Pharm Res 26: 926-935.
Jafari SM, He Y, Bhandari B (2007) Production of sub-micron emulsions by ultrasound and microfluidization techniques. J Food Eng 82: 478-488.
Jaiswal M, Dudhe R, Sharma PK (2015) Nanoemulsion: an advanced mode of drug delivery system. 3 Biotech 5: 123-127.
Karadag A, Yang X, Ozcelik B, Huang Q (2013) Optimization of preparation conditions for quercetin nanoemulsions using response surface methodology. J Agric Food Chem 61: 2130-2139.
Karbstein H, Schubert H (1995) Developments in the continuous mechanical production of oil-in-water macro-emulsions. Chem Eng Process 34: 205-211.
Kakumanue S, Tagne JB, Wilson TA, Nicolosi RJ (2011) A nanoemulsion formulation of dacarbazine reduces tumor size in a xenograft mouse epidermoid carcinoma model compared to dacarbazine suspension. Nanomed Nanotechnol 7: 277-283.
Kentish SE, Wooster TJ, Ashokkumar M, Balachandran S, Mawson R, Simons L (2008) The use of ultrasonics for nanoemulsion preparation. Innov Food Sci Emerg 9: 170-175.
Leong TSH, Wooster TJ, Kentish SE, Ashokkumar M (2009) Minimising oil droplet size using ultrasonic emulsification. Ultrason Sonochem 16: 721-727.
Li PH, Chiang BH (2012) Process optimization and stability of D-limonene-in-water nanoemulsions prepared by ultrasonic emulsification using response surface methodology. Ultrason Sonochem 19: 192-197.
Lin CC, Lin HY, Chi MH, Shen CM, Chen HW, Yang WJ, Lee MH (2014) Preparation of curcumin microemulsions with food-grade soybean oil/lecithin and their cytotoxicity on the HepG2 cell line. Food Chem 154: 282-290.
Lipinski C (2002) Poor aqueous solubility-an industry wide problem in drug discovery. Am Pharm Rev 5: 82-85.
Liu W, Sun D, Li C, Liu Q, Xu J (2006) Formation and stability of paraffin oil-in-water nano-emulsions prepared by the emulsion inversion point method. J Colloid Interface Sci 303: 557-563.

Loong NC, Basria M, Fang LF, Masoumia HR, Tripathy M, Abedi R, Abdul-Malek E (2014) Comparison of Box–Behnken and central composite designs in optimization of fullerene loaded palm-based nano-emulsions for cosmeceutical application. Ind Crops Prod 59: 309-317.

Morgan ED (1991) In: John Wiley (ed.) Chemometrics: Experimental Design, London.

Musaa SH, Basri M, Masoumia HR, Abedi R, Malek EA, Basri H, Shamsuddin AF (2013) Formulation optimization of palm kernel oil esters nanoemulsion-loaded with chloramphenicol suitable for meningitis treatment. Colloids Surf B 112: 113-119.

Rathore AS, Winkle H (2009) Quality by design for biopharmaceuticals. Nat Biotechnol 27: 26-34.

Rotem R, Heyfets A, Fingrut O, Blickstein D, Shaklai M, Flescher E (2005) Jasmonates: novel anticancer agents acting directly and selectively on human cancer cell mitochondria. Cancer Res 65: 1984-1993.

Sagitani H (1981) Making homogeneous and fine droplet o/w emulsions using nonionic surfactants. J Am Oil Chem Soc 58: 738-743.

Sharma S, Verma A, Teja BV, Shukla P, Mishra PR (2015) Development of stabilized Paclitaxel nanocrystals: in-vitro and in-vivo efficacy studies. Eur J Pharm Sci 69: 51-60.

Sood ST, Jain K, Gowthamarajan K (2014) Optimization of curcumin nanoemulsion for intranasal delivery using design of experiment and its toxicity assessment. Colloids Surf B 113: 330-337.

Stepanek P (1993) Data analysis in dynamic light scattering. In: Brown W (ed) Dynamic light scattering: The method and some applications, Oxford, p. 177-241.

Tadros TF, Izquierdo P, Esquena J, Solans C (2004) Formation and stability of nanoemulsions. Adv Colloid Interface Sci 108-109: 303-318.

Tamimi R, Sepehri H, Delphi L (2016) Experimental induction of apoptosis by salvia sahendica extract alone and in combination with doxorubicin in human prostate cancer cells, LNCaP. Int J Pharmacognosy and Phytochem Res 8: 272-283.

Tan SF, Masoumi HR, Abedi R, Stanslas J, Kirby BP, Basri M, Basri HB (2016) Ultrasonic emulsification of parenteral valproic acid-loaded nanoemulsion with response surface methodology and evaluation of its stability. Ultrason Sonochem 29: 299-308.

Wasternack C (2014) Action of jasmonates in plant stress responses and development-Applied aspects. Biotechnol Adv 32: 31-39.

Zhu Y, Zhang J, Zheng Q, Wang M, Deng W, Li Q, Firempong CK, Wang S, Tong S, Xu X, Yu J (2015) In vitro and in vivo evaluation of capsaicin-loaded microemulsion for enhanced oral bioavailability. J Sci Food Agric 95: 2678-2685.